Materials Research Bulletin 63 (2015) 164–172

Contents lists available at ScienceDirect

Materials Research Bulletin

journal homepage: www.elsevier.com/locate/matresbu

Preparation of silicon carbide SiC-based nanopowders by the aerosol-assisted synthesis and the DC thermal plasma synthesis methods

Cezary Czosnek [a,*], Mirosław M. Bućko [b], Jerzy F. Janik [a], Zbigniew Olejniczak [c], Michał Bystrzejewski [d], Olga Łabędź [d], Andrzej Huczko [d,*]

[a] AGH University of Science and Technology, Faculty of Energy and Fuels, al. A. Mickiewicza 30, 30-059 Krakow, Poland
[b] AGH University of Science and Technology, Faculty of Materials Science and Ceramics, al. A. Mickiewicza 30, 30-059 Krakow, Poland
[c] Institute of Nuclear Physics, Polish Academy of Sciences, ul. Radzikowskiego 152, 31-342 Krakow, Poland
[d] University of Warsaw, Department of Chemistry, 1 Pasteura St., 02-093 Warsaw, Poland

ARTICLE INFO

Article history:
Received 8 August 2014
Received in revised form 11 November 2014
Accepted 2 December 2014
Available online 4 December 2014

Keywords:
A. Nanostructures
A. Carbides
C. X-Ray diffraction
C. Infrared spectroscopy
C. Nuclear magnetic resonance (NMR)

ABSTRACT

Nanosized SiC-based powders were prepared from selected liquid-phase organosilicon precursors by the aerosol-assisted synthesis, the DC thermal plasma synthesis, and a combination of the two methods. The two-stage aerosol-assisted synthesis method provides at the end conditions close to thermodynamic equilibrium. The single-stage thermal plasma method is characterized by short particle residence times in the reaction zone, which can lead to kinetically controlled products. The by-products and final nanopowders were characterized by powder XRD, infrared spectroscopy FT-IR, scanning electron microscopy SEM, and ^{29}Si MAS NMR spectroscopy. BET specific surface areas of the products were determined by standard physical adsorption of nitrogen at 77 K. The major component in all synthesis routes was found to be cubic silicon carbide β-SiC with average crystallite sizes ranging from a few to tens of nanometers. In some cases, it was accompanied by free carbon, elemental silicon or silica nanoparticles. The final mesoporous β-SiC-based nanopowders have a potential as affordable catalyst supports.

1. Introduction

Silicon carbide SiC due to its high mechanical strength, semiconducting properties, chemical inertness, high-temperature stability, and good thermal conductivity has been a subject of numerous studies and growing applications. In addition to the established applications of bulk SiC, there are many utilizations that take advantage of its nanosized materials forms. For instance, SiC-based nanostructures were considered for nanoscale light emitters [1,2]. SiC membranes were shown to exhibit advantageous properties for gas separation [3–5]. SiC was also tried in diesel fuel particulate filters [6,7] and the carbide ceramic microreactors were investigated for hydrogen gas production [8,9]. In another approach, SiC was used as a support for the Ni catalyst in methane reforming to synthetic gas [10–12].

Several bottom-up precursor routes are available to prepare SiC powders. For example, they were synthesized by the carbothermal reduction method using the binary systems of the polysiloxane/phenol and polysiloxane/xylene resins [13]. Yang et al. reported a successful synthesis of SiC powders with particle sizes in the range of 0.5–1 μm by combustion synthesis from the mixtures of silicon, carbon black, and polytetrafluoroethylene powders [14]. Chemical vapor deposition synthesis in a hot-wall quartz reactor was used to make nanosized cubic β-SiC with crystallite sizes in the range of 10–30 nm using hexamethyldisilane as a precursor [15]. Du et al. described a route for making β-SiC by electric pulses discharged in liquid-phase organosilicon precursors [16]. In recent reports, microwave heating at 1200 °C of suitable mixtures of silicon, graphite, and aluminum powders yielded either α-SiC [17] or aluminum-doped β-SiC [18]. Pure or boron-doped β-SiC powders were also produced by various combustion synthesis methods [19–23].

The thermal plasma synthesis offers a highly specific way to prepare nanopowders. The attractiveness of plasma processes stems, in general, from high energy densities in the reaction zone resulting in high precursor flow rates and increased temperatures,

* Corresponding authors. Tel.: +48 12 617 2578.
E-mail addresses: czosnek@agh.edu.pl (C. Czosnek), ahuczko@chem.uw.edu.pl (A. Huczko).

http://dx.doi.org/10.1016/j.materresbull.2014.12.003
0025-5408/

with both factors causing significant reaction time reductions [24]. For instance, Kong and Pfender synthesized nanosized β-SiC powders with the arc plasma by reacting methane and silicon monoxide [24]. The resulting powders showed a bimodal distribution of particle sizes in the characteristic ranges depending on the carbon to silicon ratio. There have also been studies on using the thermal plasma for silicon carbide coatings, namely, plasma enhanced chemical vapor deposition PE CVD [25–33] or thermal plasma physical vapor deposition TP PDV [34,35]. These techniques were also used for making SiC nanoparticles [36–44].

In those investigations, organosilanes or hydrocarbon/silane precursor systems were predominantly used for both the gas phase reactions [25–33,36–38] and solid state precursor conversions [34,35,43,45]. In the present study, two liquid-phase oxygen-bearing organosilicon precursors were tried to prepare SiC nanopowders of increased specific surface area that could be considered as affordable catalyst supports. A two-stage aerosol-assisted synthesis method was used as the basic route. In the first stage, the method allows for the preparation of the raw product with spheroidal particle morphology. In the second stage, it can be either further pyrolyzed in bulk at higher temperatures or, alternatively, processed in the thermal plasma pyrolysis system to be converted to specific final products. As previously mentioned, the major advantage of the thermal plasma method is a short conversion time due to the specific reaction conditions. This, however, results in kinetically and diffusion controlled products. On the other hand, the aerosol-assisted synthesis in its second-stage of bulk pyrolysis provides sufficient time for achieving conditions close to equilibrium and, therefore, can result in different products. Proper combination of these highly automated synthesis methods, which are in some respects supplemental, is anticipated to produce still different SiC-based nanopowders.

2. Materials and methods

Two organosilicon precursors, neat hexamethyldisiloxane (HMDS) $[(CH_3)_3Si]_2O$ (Aldrich) and neat polydimethylsiloxane (PDMS) $\{-Si(CH_3)_2-O-\}_n, n_{av} = 10$ (Silikony Polskie, Sarzyna, Poland), were used as received. The first precursor is a molecular compound while the second is a mixture of relatively short polymeric chains with different lengths. From the perspective of the anticipated major SiC product, the atomic C:Si:O ratio in the precursor, *i.e.*, 6:2:1 for HMDS and 2:1:1 for PDMS is a crucial factor that determines the efficiency of carbothermal reduction and, consequently, the composition of intermediate and final products.

First, raw powders were prepared by the aerosol-assisted synthesis method in the experimental set-up shown in Fig. 1. The details of the method were published elsewhere [46]. A mist of neat hexamethyldisiloxane was generated by an ultrasound generator whereas in the case of polydimethylsiloxane, due to its high surface tension retarding the ultrasonic aerosol formation, a spray generator (ATM 220, Topas, Germany) was used. The precursor mist was transported in a stream of argon gas with a flow rate 3 L/min to the ceramic tube reactor placed in an electric furnace, which was preheated to 1200 °C. The powder product that was formed inside the reactor was collected on the exit nylon filter. The as-prepared products were black free-flowing powders. Due to incomplete carbothermal reduction/carbide formation, such raw products usually contain glassy silicon oxycarbide SiO_xC_y and/or free carbon and silica [47]. In order to eliminate the remaining oxygen and promote SiC formation and crystallization, an additional treatment of the raw powder at an elevated temperature was necessary. In the follow-up stage, the pyrolysis of the powder at 1650 °C under flowing argon, 1 L/min, was carried out, as it is typically done in the aerosol-assisted synthesis, to yield the final product.

In parallel experiments, each raw product was additionally treated in a DC argon plasma stream, in the experimental set-up shown in Fig. 2 that was described in details elsewhere [48]. The raw powder obtained from the aerosol-assisted synthesis was fed directly into the plasma stream of the reaction chamber at a feeding rate of a few grams per minute, using a home-made fluidized-bed feeder with argon gas as the transporting medium. The thermal plasma was generated by a DC arc discharge. Additionally, as a reference reaction system, the argon plasma set-up was used to generate powders directly from the liquid polydimethylsiloxane. In this case, the powder feeder was replaced by a feeder suitable for liquid precursors. The experiments were carried out at the input power 20 kW, argon gas flow rate 2.4 m^3/h, and the feeding rate of precursor 16 g/min.

The overall scheme of performed experiments and resulting samples, including the sequence of applied synthesis steps/stages, type of raw products, and realized pathways to final nanopowders is shown in Fig. 3.

All powders were characterized by powder XRD (X'Pert Pro Panalytical, Cu Kα source), scanning electron microscopy SEM (Hitachi, model S-4700 and Zeiss, model ULTRA plus), FT-IR spectroscopy (Nicolet 380, Thermo Electron Corporation, KBr pellets), and in selected cases, solid-state ^{29}Si MAS NMR spectroscopy (Tecmag Apollo spectrometer at 59.515 MHz, Bruker HP-WB MAS probe). BET specific surface areas of the samples were determined by the standard physical adsorption of nitrogen at 77 K on Micromeritics Gemini **V** 2380.

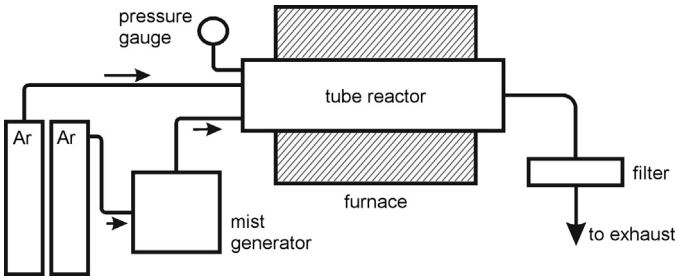

Fig. 1. Set-up for aerosol-assisted raw powder generation.

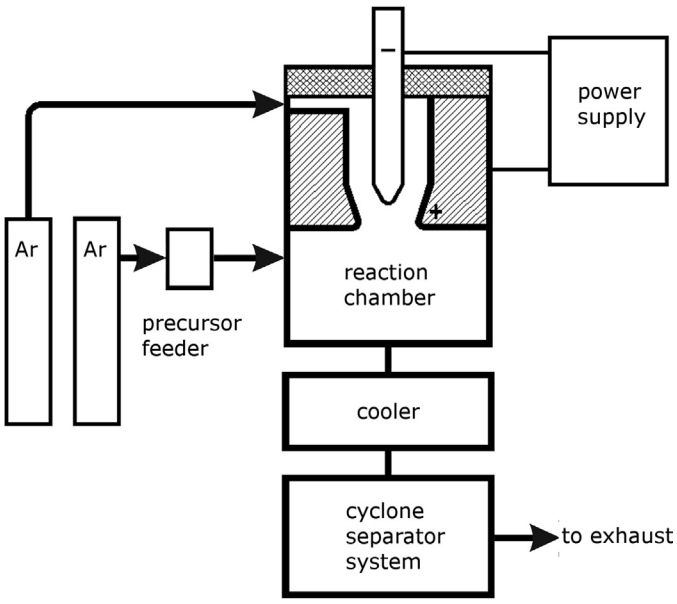

Fig. 2. DC thermal plasma jet system.

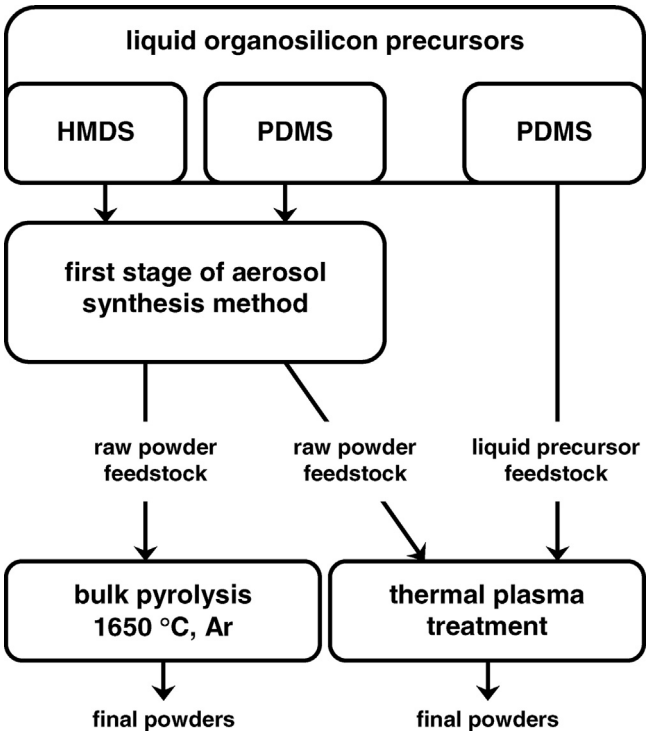

Fig. 3. Scheme of precursors conversion to SiC-based nanopowders.

3. Results and discussion

The successful chemistry behind the carbothermal reduction of oxygen-bearing organosilicon compounds under the neutral gas atmosphere relies on three main processes. First, thermally driven precursor decomposition at elevated temperatures has to occur. Second, the high affinity of the resulting carbonaceous species to react with Si-O-bearing decomposition by-products with the formation of gaseous carbon oxides leads *via* carbothermal reduction to oxygen-deprived silicon species. And third, given a sufficient supply of carbon species and appropriately high temperatures, silicon should react with still available carbon to form silicon carbide SiC. However, this somewhat simplified reaction pathway has to take into account a possibility of amorphous oxycarbide SiO_xC_y formation as well as of free carbon C and silica SiO_2 as composite components at moderate temperatures up to 1400 °C [47,49,50]. This complication is directly linked to the chemical composition of the precursor which can be conveniently described by its C:Si:O atomic ratio.

In this regard, hexamethyldisiloxane, C:Si:O = 6:2:1, contains a sufficient amount of constitutional carbon atoms for both the carbothermal reduction/oxygen removal and formation of SiC. In the case of polydimethylsiloxane, which is an inexpensive organosilicon precursor with C:Si:O = 2:1:1, the relative amount of carbon atoms only theoretically allows for the formation of SiC and elimination of oxygen under highly favorable time/diffusion conditions. In some cases, however, a local availability of carbon may be insufficient for efficient oxygen removal and, consequently, oxygen-bearing silicon oxycarbide SiO_xC_y and/or silica SiO_2 could appear in the products.

3.1. Synthesis of raw powders

The raw powder products were prepared from the liquid organosilicon precursors by the aerosol-assisted synthesis method at 1200 °C using argon as a neutral gas carrier. The SEM micrographs of the products show a typical particle morphology for the method – the particles are spheroidal and often fused together (Fig. 4). It should be noted that nanopowders most often form extensively agglomerated assemblies of amorphous by-products or product crystallites, so that *particle* refers to an entire agglomerate, not necessarily in the nanosized range. The specific feature of the aerosol-assisted method is the formation of raw powders consisting of spherical particles. This effects the way the final product forms and, subsequently, crystallizes to yield agglomerated nanocrystallites in the second-stage treatment.

After the first stage, the products exhibit merely weak crystalline characteristics if any, as demonstrated by the XRD patterns (Fig. 5). In the pattern for the product from hexamethyldisiloxane (HMDS), a broad halo located at *ca.* $2\theta = 35°$ (Fig. 5A) could be linked to emerging β-SiC (JCPDS-ICDD No. 29-1129). In contrast to the HMDS-derived product, the powder from PDMS appears to be entirely amorphous (Fig. 5B).

The FT-IR spectra for the raw products are shown in Fig. 6. They are remarkably similar in the characteristic spectral ranges. The absorption bands corresponding to the expected silicon moieties, *i.e.*, stretching mode of Si—O bonds at *ca.* 1060 cm^{-1} and that of Si—C bonds at 840 cm^{-1} are observed. An additional band appears at *ca.* 464 cm^{-1} which is probably due to the bending vibrations of Si—O bonds (Fig. 6B). The remaining weak absorption bands at *ca.* 3430 cm^{-1} and 1600 cm^{-1} correspond to the stretching and bending vibrations of O—H groups, respectively, in adventitiously adsorbed water molecules. In our related study, we pointed out that at relatively low synthesis temperatures in the range

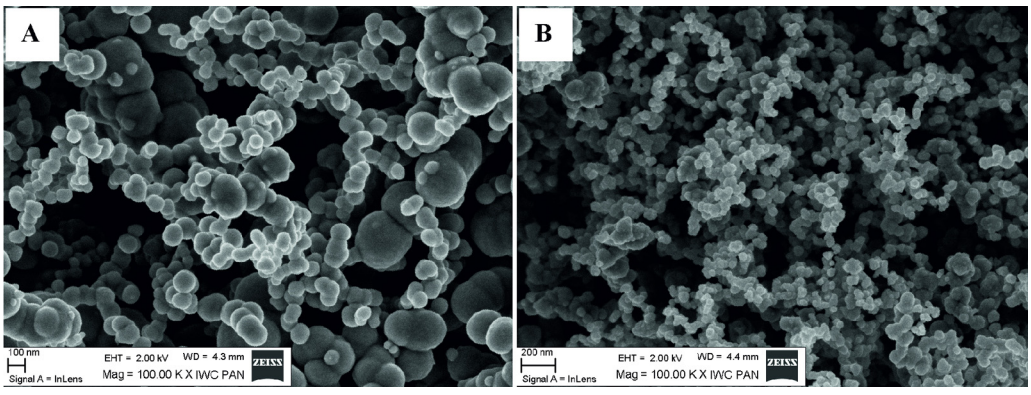

Fig. 4. SEM images of raw powders prepared with the aerosol-assisted synthesis method at 1200 °C, Ar, from: A – HMDS, B – PDMS.

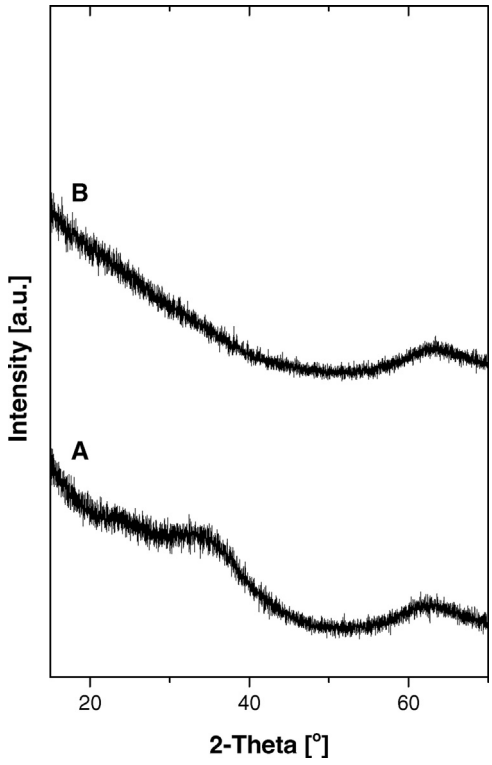

Fig. 5. XRD patterns for raw powders prepared with the aerosol-assisted synthesis method at 1200 °C, Ar, from: A – HMDS, B – PDMS.

1200–1400 °C, it was possible to prepare products that contain amorphous/glassy silicon oxycarbide SiO_xC_y, in which a certain number of four-coordinated carbon atoms were replaced by two-coordinated oxygen atoms [47]. Therefore, it is difficult to say on the basis of the FT-IR results only whether such oxycarbides are formed or not in the present study.

An additional insight into this question is provided by ^{29}Si MAS NMR spectroscopy, a technique sensitive to the local chemical environment of silicon atoms. In general, local environments denoted in short as SiC_4, SiC_3O, SiC_2O_2, $SiCO_3$, and SiO_4 will be manifested by distinct peaks with the first one typical for SiC, the last characteristic for SiO_2, and the remaining assigned to various combinations of oxygen and carbon around silicon centers in SiO_xC_y. The corresponding peak positions for SiC_4, SiC_3O, SiC_2O_2, $SiCO_3$, and SiO_4 units are *ca.* −16 ppm, 1 ppm, −34 ppm, −72 ppm, and −107 ppm, respectively [49]. The MAS NMR spectrum for the raw powder from hexamethyldisiloxane is dominated by a broad peak extending from *ca.* 17 ppm to −55 ppm with maximum at about −15 ppm, which reasonably corresponds to the SiC_4 units in β-SiC (Fig. 7A). There is a slight discrepancy between our data and the available literature references [51]. It can be explained by the presence of overlapping additional peaks from the SiC_2O_2 (−34 ppm) and SiC_3O units (1 ppm) in the silicon oxycarbide that could plausibly be formed under such conditions. A considerably smaller peak is observed at *ca.* −67 ppm which corresponds to the $SiCO_3$ units. Due to relatively low signal to noise ratio, it is difficult to confirm in this case the presence of SiO_4 units in SiO_2.

The NMR spectrum for the raw powder prepared from polydimethylsiloxane (Fig. 7B) exhibits essentially the same peaks. However, the peak intensity at −70 ppm corresponding to the $SiCO_3$ units is increased. A peak of low intensity at −107 ppm for the SiO_4 units is now convincingly detected, confirming that some silica is formed in addition to the main oxycarbide product. This observation can be explained by the C:Si:O atomic ratios in the precursors and the relative deficiency of carbon in the case of polydimethysiloxane, which favors the oxygen retention in the derived products.

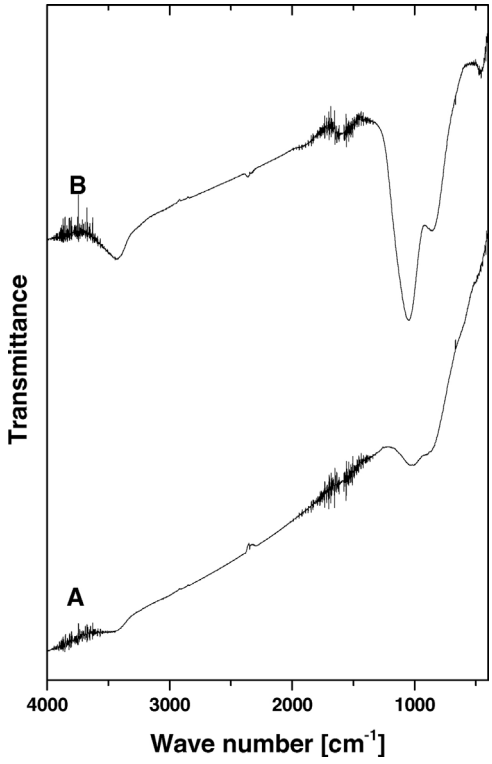

Fig. 6. FT-IR spectra for raw powders prepared with the aerosol-assisted synthesis method at 1200 °C, Ar, from: A – HMDS, B – PDMS.

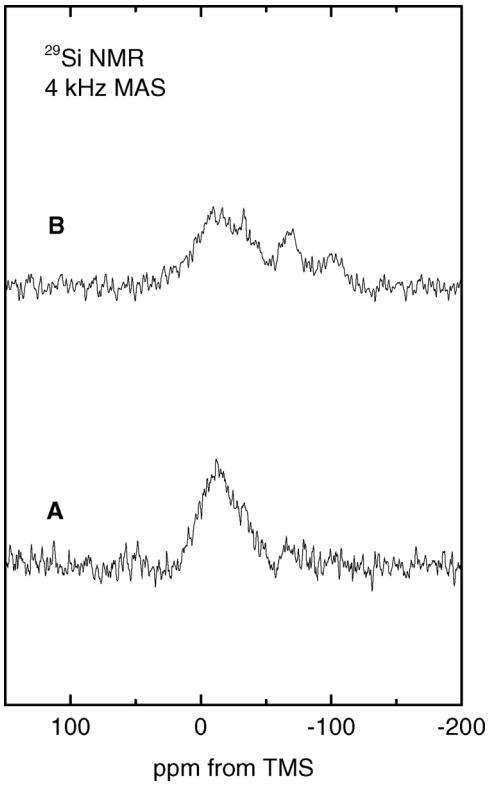

Fig. 7. ^{29}Si MAS NMR spectra for raw powders prepared with the aerosol-assisted synthesis method at 1200 °C, Ar, from: A – HMDS, B – PDMS.

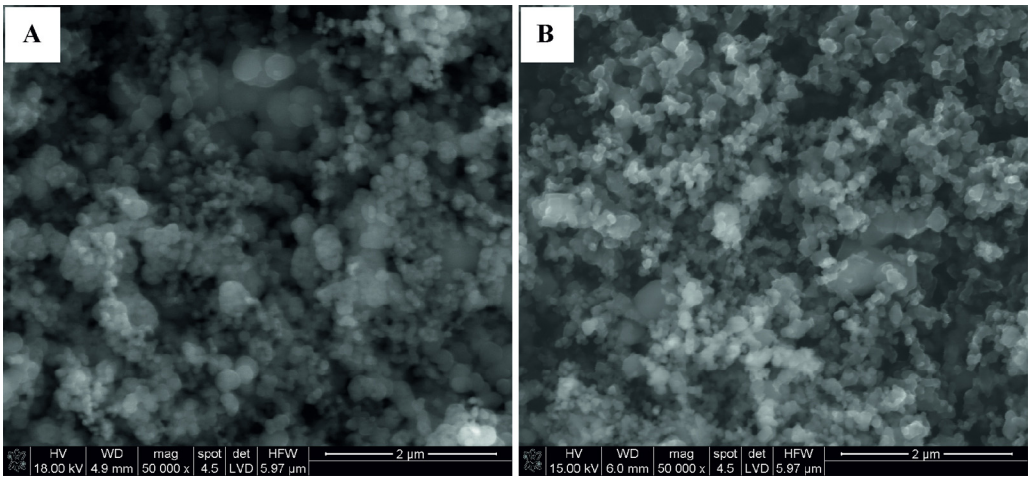

Fig. 8. SEM images of final powders obtained after additional bulk pyrolysis at 1650 °C, Ar, of raw powders from: A – HMDS and B – PDMS.

3.2. Second stage pyrolysis of raw powders

The raw powders prepared in the first stage of the aerosol-assisted synthesis were subjected to further pyrolysis by two different methods of thermal treatment, namely, by bulk pyrolysis of powders in a tube furnace at 1650 °C, or under the conditions of DC thermal plasma. Both methods of the heat treatment were carried out in the argon atmosphere. Under such conditions, chemically bound oxygen in SiO_xC_y and/or SiO_2 is expected to undergo an efficient carbothermal reduction by carbon available either from silicon oxycarbide and/or dispersed as a free excess carbon phase, resulting in pure SiC or C/SiC composite nanopowders.

It is worth to point out that both these highly automated methods inherently lead to some material losses that are related rather to the process yield than to the chemical reaction yield. In the aerosol synthesis, the exit section of the ceramic tube reactor is gradually covered with a thin powder layer that grows thicker with time/consecutive runs, until reaching a limited working thickness. Once the tube is "conditioned", subsequent runs proceed without virtually any product losses of this type. Similarly, there are parts of the thermal plasma synthesis apparatus from which it is difficult to recover the product. It is retained there during the first run, mainly. The overall process yield for a single run in either of the methods is estimated at 70–80% but it can be higher if consecutive runs are made to prepare larger quantities of the product.

The characteristic SEM images of the final products after the bulk pyrolysis at 1650 °C, Ar, are presented in Fig. 8. The powder from HDMS preserves the initial particle morphology formed in the first stage of the synthesis (Fig. 8A). The bimodal size distribution of the particles in the raw powders (Fig. 4) appears to survive the high temperature treatment. Most of the spheroidal particles possess a blackberry-like appearance. Somewhat different particle morphology is observed in the PDMS-derived powder (Fig. 8B). The spheroidal morphology of the particles is frequently deformed and a closer inspection reveals a number of larger particles with well-developed crystal facets. This suggests that under such pyrolysis conditions the crystal growth takes place although most of the crystallites appear as nanocrystalline aggregates.

The SEM images of the powders prepared from HDMS and PDMS by the aerosol-assisted synthesis after the second-stage treatment in the DC thermal plasma are presented in Fig. 9A and B, respectively. The particle morphology is, generally, very much like from the first stage of the aerosol synthesis. However, in this case the particles seem to be less deformed (compare with Fig. 8). Interestingly, the powders from PDMS (Figs. 8 and 9B) after the second stage of pyrolysis contain much more deformed particles in comparison with the appropriate products from HMDS, independently of the pyrolysis method. This probably results from specific thermochemical changes yielding certain by-products that show an apparent partial melting [46]. This, in turn, could be related to

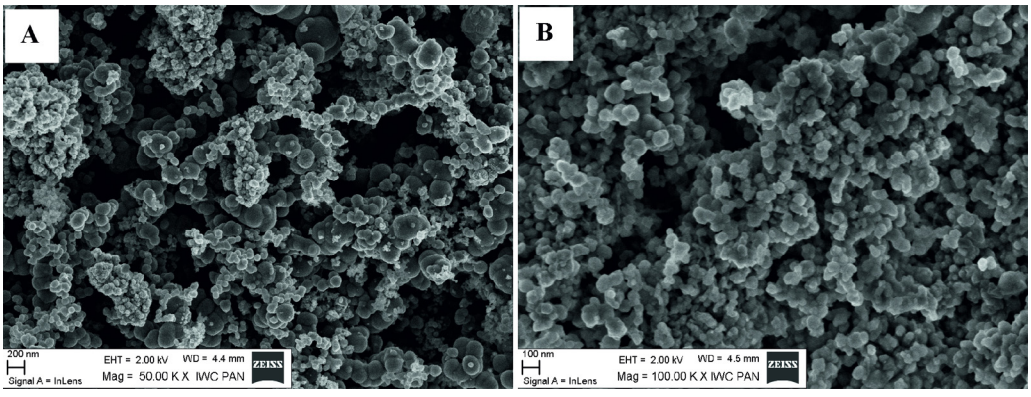

Fig. 9. SEM images of powders obtained after additional treatment in DC thermal plasma of raw powders from: A – HMDS and B – PDMS.

the C:Si atomic ratio in the precursors (3:1 in HMDS and 2:1 in PDMS). Due to higher relative deficiency of carbon in PDMS, the formation of elemental silicon Si (m. p. 1414 °C) or silica SiO_2 (m. p. around 1670 °C) is feasible. In fact, such a conclusion is consistent with the relevantXRD results (*vide infra*), especially, for the powder after the pyrolysis in plasma stream.

The diffraction patterns for powders after the second stage of the heat treatment are shown in Fig. 10. The HMDS patterns after the bulk pyrolysis in the tube furnace and after the treatment in the DC thermal plasma are shown in Fig. 10A and B, respectively, whereas the corresponding PDMS patterns in Fig. 10C and D. Additionally, the diffraction pattern of the powder prepared by a direct conversion of liquid PDMS in a single-stage conversion carried out in the DC thermal plasma is presented in Fig. 10E. The major features in all these patterns are the diffraction peaks attributed to the dominant cubic phase β-SiC. A small shoulder at *ca.* 34° is assigned to the minor hexagonal polytype α-SiC which frequently accompanies the formation of nanocrystalline β-SiC from chemical precursors. The average crystallite sizes of the β-SiC phase as calculated from the Scherrer equation for the samples shown in Fig. 10A and D are, respectively, 32 nm, 26 nm, 24 nm, and 18 nm. The detailed examination of the diffraction pattern shape for the powder from the direct pyrolysis of PDMS in thermal plasma (Fig. 10E) suggests a bimodal size distribution of β-SiC crystallites. The crystallite size calculations for this sample applied to the deconvoluted strongest (1 1 1) diffraction peak at 35.6° yield the average sizes of 15 nm and 2 nm in the amounts of *ca.* 30% and 70%, respectively. It is worth to note that the average crystallite size of β-SiC formed from polydimethylsiloxane is smaller than that from hexamethyldisiloxane irrespective of the second-stage heat treatment method. Moreover, the powder that was thermally treated in the DC thermal plasma consists of smaller β-SiC crystallites than the powder from the respective bulk pyrolysis in the tube furnace. The last observation can be explained by different residence times of particles in the high temperature zone of the two heat treatment methods – a much longer residence time of bulk pyrolysis at 1650 °C favors the crystal growth and the formation of larger crystallites.

Interestingly, a considerable amount of elemental silicon Si in addition to β-SiC is observed in the PDMS powder that was treated in the DC thermal plasma (Fig. 10D). On the other hand, silicon is not detected in the product from the direct conversion of liquid PDMS in the thermal plasma under otherwise the same conditions. This suggests that significant differences occur in the course of relevant transformations. Due to the C:Si:O ratios in the precursors, *i.e.*, 6:2:1 for HMDS and 2:1:1 for PDMS, the raw powders from the aerosol-assisted synthesis have different elemental and constitutional compositions. This is confirmed by the ^{29}Si MAS NMR determinations and corroborated by the FT-IR results (Figs. 6 and 7). The black raw powders after the first stage of the aerosol synthesis at 1200 °C contain the SiO_xC_y species and free excess carbon from the decomposition of methyl groups. Additionally, the raw powder from HMDS contains some amorphous SiC while that from PDMS has SiO_2 as seen in ^{29}Si MAS NMR (Fig. 7B) and FT-IR spectroscopy (Fig. 6). The predominant thermochemical change leading in the second stage to β-SiC can, in principle, be described by carbothermal reduction

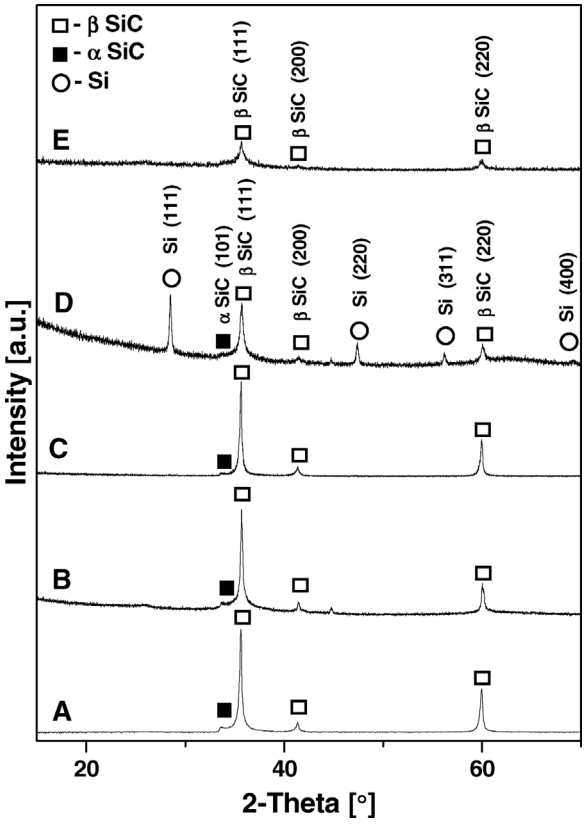

Fig. 10. XRD patterns for final powders obtained after additional treatment of raw powders from the aerosol-assisted synthesis – precursor (treatment): A – HMDS (bulk pyrolysis, 1650 °C, Ar), B – HMDS (DC thermal plasma), C – PDMS (bulk pyrolysis, 1650 °C, Ar), D – PDMS (DC thermal plasma), and E – powder prepared by direct conversion of liquid PDMS in DC thermal plasma. The crystalline phases were identified based on JCPDS-ICDD reference data, *i.e.*, β-SiC (JCPDS-ICDD: 29-1129), α-SiC (JCPDS-ICDD: 01-072-0018), Si (JCPDS-ICDD: 00-027-1402).

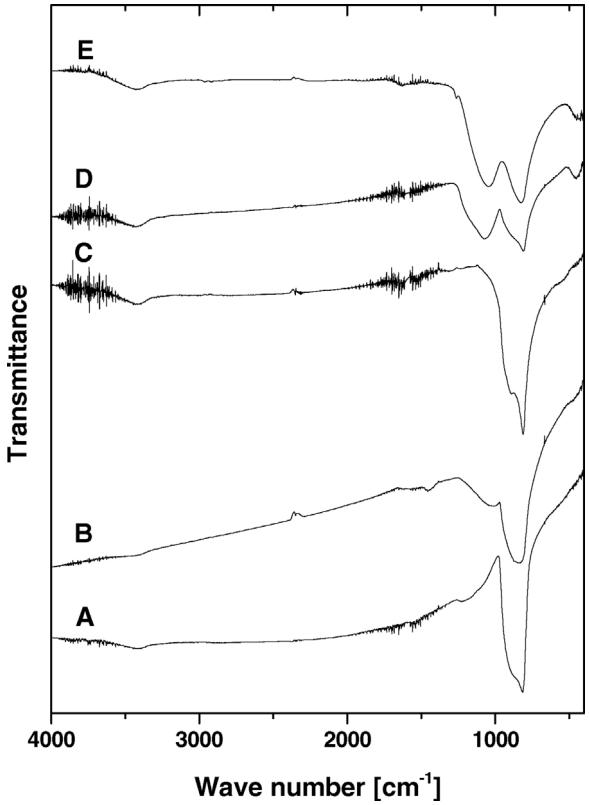

Fig. 11. FT-IR spectra for final powders obtained after additional treatment of raw powders from the aerosol-assisted synthesis – precursor (treatment): A – HMDS (bulk pyrolysis, 1650 °C, Ar), B – HMDS (DC thermal plasma), C – PDMS (bulk pyrolysis, 1650 °C, Ar), D – PDMS (DC thermal plasma), and E – powder prepared by direct conversion of liquid PDMS in DC thermal plasma.

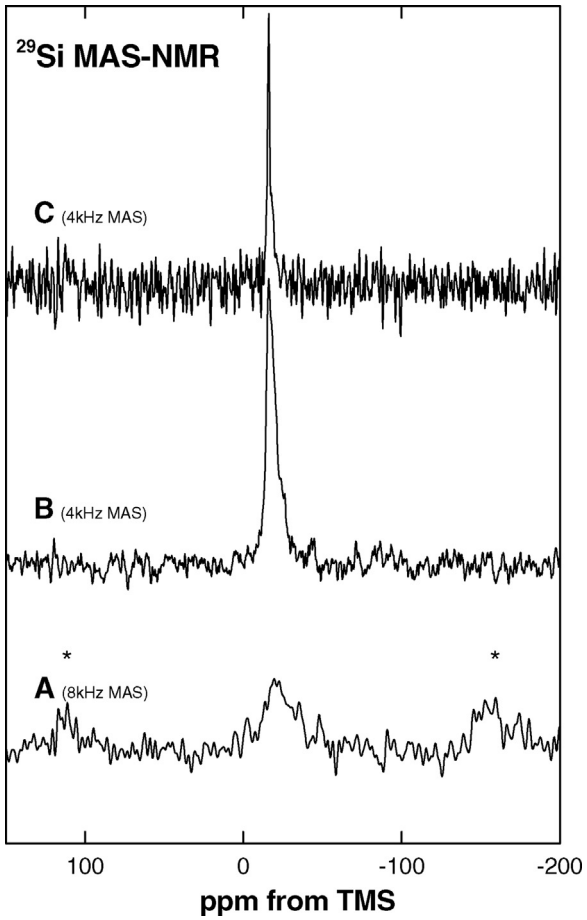

Fig. 12. ^{29}Si MAS NMR spectra for selected final powders after additional treatment of raw powders from the aerosol-assisted synthesis – precursor (treatment): A – HMDS (DC thermal plasma), B – HMDS (bulk pyrolysis, 1650 °C, Ar), C – PDMS (bulk pyrolysis, 1650 °C, Ar). The peaks marked by asterisks in the A spectrum are the spinning sidebands.

of the type $SiO_2 + 2C \rightarrow SiC + CO_2\uparrow$ which occurs in both raw powders. In the case of PDMS, the elemental Si is likely formed during an incomplete carbothermal reduction of the type $SiO_2 + C \rightarrow Si + CO_2\uparrow$. It becomes significant under turbulent flow conditions of the thermal plasma method coupled with the deficiency of available carbon. Moreover, the way the raw powder is transported in argon to the plasma chamber is thought to reduce the physical contact of carbon particles with the SiO_2 and/or SiO_xC_y particles, creating conditions that favor the formation of elemental Si. This can be compared with the outcome of the direct pyrolysis of liquid PDMS in the DC thermal plasma and exclusive formation of β-SiC in the lowest nanosized regime as confirmed by the XRD results (Fig. 10E).

Fig. 11 shows the FT-IR spectra of all final powders arranged in the same order as the XRD patterns in Fig. 10. All spectra exhibit a band at *ca.* 820 cm^{-1} which is typical for the Si—C bond stretches in SiC. Additionally, a relatively strong absorption band at *ca.* 1060 cm^{-1} that is characteristic for the Si—O stretches is observed in the spectra presented in Fig. 11D and E, corresponding to the PDMS-derived powder obtained after the heat treatment in thermal plasma of the raw product from aerosol synthesis and the powder from the single-step direct pyrolysis of liquid PDMS in the DC thermal plasma, respectively. No such band is observed for the final powder prepared from the PDMS-derived raw product after the bulk pyrolysis in the tube furnace (Fig. 11C). This suggests that advantageous conditions exist in the latter method, including sufficient amounts of carbon and suitably long reaction time to yield oxygen-deprived products, mainly, SiC. A similar spectrum for the final powder from HMDS after the second-stage bulk pyrolysis is seen as well, confirming the high specificity of such a two-stage synthesis method.

Fig. 12 shows the ^{29}Si MAS NMR spectra for the selected samples, *i.e.*, powder from HDMS obtained after the second-stage treatment in thermal plasma (Fig. 12A) and powders from HDMS and PDMS obtained after the second-stage bulk pyrolysis in tube furnace (Fig. 12B and C, respectively). One narrow peak at *ca.* −16 ppm assigned to crystalline β-SiC is observed in Fig. 12B and C, which is consistent with the XRD results. Broad spinning sidebands in the frequency range extending from 300 to −300 ppm (not shown) are present in the spectrum shown in Fig. 12 A. They are due to an inhomogeneous broadening that can be caused by some paramagnetic impurities. This explains much smaller intensity of the central band at −16 ppm because the integral over the entire spectrum including the sidebands is proportional to the Si content in the sample. In spite of the poor signal to noise ratio in the spectrum, a small asymmetry of the central band is apparent. It suggests that apart from the dominant SiC_4 units (in SiC), some SiC_2O_2 moieties can be present (reported resonance at −35 ppm). This agrees with the FT-IR data that show besides the main peak at 820 cm^{-1} corresponding to SiC a broad shoulder at *ca.* 1100 cm^{-1} as well. It is indicative of some Si—O bonds in the product, probably in the amorphous SiO_xC_y component. All this is consistent with the notion that despite the abundance of carbon in the precursor, the operating conditions in the DC thermal plasma method are not effective in removing all oxygen to yield pure SiC or C/SiC composites: the residence time and the particle-to-particle contact time are too short to complete the reactions taking place, mostly, in the solid state.

The BET specific surface areas, S_{BET}, of final powders were determined by standard low temperature nitrogen adsorption revealing some differences among them (Table 1). The lowest area, 16 m^2/g, is for the PDMS-derived powder after the bulk pyrolysis in the tube furnace which is consistent with the presence of relatively large particles of SiC. The product from HMDS prepared by the same method has the surface area of 49 m^2/g, three times bigger, and this can likely be attributed to the presence of free carbon in this composite powder. For the products prepared from the two precursors by the coupled aerosol-assisted/plasma method, the larger surface area of 77 m^2/g is for the powder from PDMS. This can be due to the presence of β-SiC crystallites with the smallest crystallite sizes among the samples and, additionally, to the fine forms of crystalline silicon and amorphous silicon oxycarbide in the PDMS-derived powder. The nitrogen adsorption/desorption curves (not shown) are consistent with the mesoporous

Table 1
BET specific surface areas of final powders.

Precursor	S_{BET} [m^2/g]	
	Two-stage aerosol-assisted synthesis	Coupled aerosol-assisted/plasma synthesis
Hexamethyldisiloxane (HMDS)	49	32
Polydimethylsiloxane (PDMS)	16	77

characteristics of powders which is advantageous for the particle surface modifications.

4. Conclusions

Two individual methods and their coupled version for the conversion of selected organosilicon precursors toward SiC-based nanopowders were compared, namely, the aerosol-assisted and the DC thermal plasma methods. The composition of final powders can be related to the specifics of the applied method. The two-stage aerosol-assisted synthesis provides in the second stage of bulk pyrolysis at 1650 °C conditions that are close to equilibrium and the appropriate products. On the other hand, the DC thermal plasma method is characterized by relatively short particle residence times and limited solid particles interactions in the plasma stream. It leads to the products that are kinetically and diffusion controlled. The chemistry behind the conversion of oxygen-bearing organosilicon compounds to SiC or C/SiC is rather complex and it includes a viable silicon oxycarbide SiO_xC_y by-product formation. Therefore, a choice of one of the two synthesis methods or their coupled version will warrant the preferred nature of the final nanopowder at the optimized reaction time. An additional flexibility of this approach stems from the pool of available liquid precursors that can be used. The prepared SiC-based nanopowders are mesoporous of increased specific surface areas with capacity to be utilized as catalyst supports.

Acknowledgments

C. Czosnek and J.F. Janik acknowledge a financial support from the AGH University of Science and Technology, Grant No. 11.11.210.213; A. Huczko acknowledges a financial support from the Polish National Science Center (NCN), Grant No. 2011/03/B/ST5/03526.

References

[1] J.Y. Fan, X.L. Wu, P.K. Chu, Low-dimensional SiC nanostructures: fabrication, luminescence, and electrical properties, Prog. Mater. Sci. 51 (2006) 983–1031.
[2] N. Zhang, D.J. Dai, W.X. Zhang, J.Y. Fan, Photoluminescence and light reabsorption in SiC quantum dots embedded in binary-polyelectrolyte solid matrix, J. Appl. Phys. 112 (2012) 094315.
[3] B. Elyassi, M. Sahimi, T.T. Tsotsis, Silicon carbide membranes for gas separation applications, J. Membr. Sci. 288 (2007) 290–297.
[4] W.X. Deng, X.H. Yu, M. Sahimi, T.T. Tsotsis, Highly permeable porous silicon carbide support tubes for the preparation of nanoporous inorganic membranes, J. Membr. Sci. 451 (2014) 192–204.
[5] R.J. Ciora, B. Fayyaz, P.K.T. Liu, V. Suwanmethanond, R. Mallada, M. Sahimi, T.T. Tsotsis, Preparation and reactive applications of nanoporous silicon carbide membranes, Chem. Eng. Sci. 59 (2004) 4957–4965.
[6] C. Benaqqa, M. Gomina, A. Beurotte, M. Boussuge, B. Delattre, K. Pajot, E. Pawlak, F. Rodrigues, Morphology physical, thermal and mechanical properties of the constitutive materials of diesel particulate filters, Appl. Therm. Eng. 62 (2014) 599–606.
[7] D. O'Sullivan, M.J. Pomeroy, S. Hampshire, M.J. Murtagh, Degradation resistance of silicon carbide diesel particulate filters to diesel fuel ash deposits, J. Mater. Res. 19 (2004) 2913–2921.
[8] I.-K. Sung, C.M. Mitchell, D.-P. Kim, P.J.A. Kenis, Tailored macroporous SiCN and SiC structures for high-temperature fuel reforming, Adv. Funct. Mater. 15 (2005) 1336–1342.
[9] C.M. Mitchell, D.-P. Kim, P.J.A. Kenis, Ceramic microreactors for on-site hydrogen production, J. Catal. 241 (2006) 235–242.
[10] H. Liu, S. Li, S. Zhang, J. Wang, G. Zhou, L. Chen, X. Wang, Catalytic performance of novel Ni catalysts supported on SiC monolithic foam in carbon dioxide reforming of methane to synthesis gas, Catal. Commun. 9 (2008) 51–54.
[11] J.M. García-Vargas, J.L. Valverde, A. de Lucas-Consuegra, B. Gómez-Monedero, P. Sánchez, F. Dorado, Precursor influence and catalytic behaviour of Ni/CeO_2 and Ni/SiC catalysts for the tri-reforming process, Appl. Catal. A-Gen. 431–432 (2012) 49–56.
[12] H. Liu, S. Li, S. Zhang, L. Chen, G. Zhou, J. Wang, X. Wang, Catalytic performance of monolithic foam Ni/SiC catalyst in carbon dioxide reforming of methane to synthesis gas, Catal. Lett. 120 (2008) 111–115.
[13] K.J. Kim, S. Lee, J.H. Lee, M.H. Roh, K.Y. Lim, Y.W. Kim, Structural and optical characteristics of crystalline silicon carbide nanoparticles synthesized by carbothermal reduction, J. Am. Ceram. Soc. 92 (2009) 424–428.
[14] K. Yang, Y. Yang, Z.M. Lin, J.T. Li, J.S. Du, Mechanical-activation-assisted combustion synthesis of SiC powders with polytetrafluoroethylene as promoter, Mater. Res. Bull. 42 (2007) 1625–1632.
[15] A. Gupta, C. Jacob, A simple method to synthesize nano-sized 3C-SiC powder using hexamethyldisilane in a CVD reactor, Mater. Sci. Forum 527–529 (2006) 767–770.
[16] K. Du, H. Yang, R. Wei, M. Li, Q. Yu, W. Fu, N. Yang, H. Zhu, Y. Zeng, Electric-pulse discharge as a novel technique to synthesize β-SiC nano-crystallites from liquid-phase organic precursors, Mater. Res. Bull. 43 (2008) 120–126.
[17] J. Kuang, W. Cao, S. Elder, Synthesis of α-SiC particles at 1200 °C by microwave heating, Powder Technol. 247 (2013) 106–111.
[18] H.B. Jin, M.S. Cao, W. Zhou, S. Agathopoulos, Microwave synthesis of Al-doped SiC powders and study of their dielectric properties, Mater. Res. Bull. 45 (2010) 247–250.
[19] L.H. Wang, Y. Peng, X.B. Hu, X.G. Xu, Combustion synthesis of high purity SiC powder by radio-frequency heating, Ceram. Int. 39 (2013) 6867–6875.
[20] K. Yang, J.T. Li, L. Qi, H. Zhang, D. Zhang, H. Yan, Combustion synthesis of SiC nanosized powders at low nitrogen pressure, Powder Metall. 54 (2011) 529–532.
[21] M. Soszyński, O. Łabędź, A. Huczko, Combustion synthesis of Si-related crystalline nanostructures, J. Cryst. Growth 401 (2014) 445–448.
[22] Z. Yermekova, Z. Mansurov, A. Mukasyan, Influence of precursor morphology on the microstructure of silicon carbide nanopowder produced by combustion syntheses, Ceram. Int. 36 (2010) 2297–2305.
[23] X.L. Su, W.C. Zhou, Z.M. Li, F. Luo, H.L. Du, D.M. Zhu, Preparation and dielectric properties of B-doped SiC powders by combustion synthesis, Mater. Res. Bull. 44 (2009) 880–883.
[24] P.C. Kong, E. Pfender, Formation of ultrafine β-silicon carbide powders in an argon thermal plasma jet, Langmuir 3 (1987) 259–265.
[25] N.P. Rao, N. Tymiak, J. Blum, A. Neuman, H.J. Lee, S.L. Girshick, P.H. McMurry, J. Heberlein, Hypersonic plasma particle deposition of nanostructured silicon and silicon carbide, J. Aerosol Sci. 29 (1998) 707–720.
[26] J. Heberlein, O. Postel, S. Girshick, P. McMurry, W. Gerberich, D. Iordanoglou, F. Di Fonzo, D. Neumann, A. Gidwani, M. Fan, N. Tymiak, Thermal plasma deposition of nanophase hard coatings, Surf. Coat. Tech. 142–144 (2001) 265–271.
[27] J. Hafiz, R. Mukherjee, X. Wang, J.V.R. Heberlein, P.H. McMurry, S.L. Girshick, Analysis of nanostructured coatings synthesized by ballistic impaction of nanoparticles, Thin Solid Films 515 (2006) 1147–1151.
[28] A.R. Beaber, L.J. Qi, J. Hafiz, P.H. McMurry, J.V.R. Heberlein, W.W. Gerberich, S.L. Girshick, Nanostructured SiC by chemical vapor deposition and nanoparticle impaction, Surf. Coat. Tech. 202 (2007) 871–875.
[29] F. Liao, S. Park, J.M. Larson, M.R. Zachariah, S.L. Girshick, High-rate chemical vapor deposition of nanocrystalline silicon carbide films by radio frequency thermal plasma, Mater. Lett. 57 (2003) 1982–1986.
[30] Y. Kojima, Y. Andoo, M. Doi, Thermal plasma chemical vapor deposition of SiC, ISIJ Int. 35 (1995) 1381–1387.
[31] A. Soum-Glaude, L. Thomas, E. Tomasella, J.M. Badie, R. Berjoan, Selective effect of ion/surface interaction in low frequency PACVD of SiC:H films: Part A. Gas phase considerations, Surf. Coat. Tech. 200 (2005) 855–858.
[32] H. Sachdev, P. Scheid, Formation of silicon carbide and silicon carbonitride by RF-plasma CVD, Diamond Relat. Mater. 10 (2001) 1160–1164.
[33] S.L. Girshick, J. Hafiz, Thermal plasma synthesis of nanostructured silicon carbide films, J. Phys. D: Appl. Phys. 40 (2007) 2354–2360.
[34] X.H. Wang, K. Eguchi, C. Iwamoto, T. Yoshida, High-rate deposition of nanostructured SiC films by thermal plasma PVD, Sci. Technol. Adv. Mat. 3 (2002) 313–317.
[35] X.H. Wang, K. Eguchi, C. Iwamoto, T. Yoshida, Ultrafast thermal plasma physical vapor deposition of thick SiC films, Sci. Technol. Adv. Mat. 4 (2003) 159–165.
[36] F. Gitzhofer, Induction plasma synthesis of ultrafine SiC, Pure Appl. Chem. 68 (1996) 1113–1120.
[37] H.F. Lin, J.A. Gerbec, M. Sushchikh, E.W. McFarland, Synthesis of amorphous silicon carbide nanoparticles in a low temperature low pressure plasma reactor, Nanotechnology 19 (2008) 325601–325608.
[38] S. Klein, M. Winterer, H. Hahn, Reduced-pressure chemical vapor synthesis of nanocrystalline silicon carbide powders, Chem. Vap. Deposition 4 (1998) 143–149.
[39] Y. Inoue, Y. Nariki, K. Tanaka, Mechanism of production of ultra-fine silicon carbide powder by arc plasma irradiation of silicon bulk in methane-based atmospheres, J. Mater. Sci. 24 (1989) 3819–3823.
[40] C.M. Hollabaugh, D.E. Hull, L.R. Newkirk, J.J. Petrovic, R.F.-plasma system for the production of ultrafine, ultrapure silicon carbide powdetr, J. Mater. Sci. 18 (1983) 3190–3194.
[41] M. Vennekamp, I. Bauer, M. Groh, E. Sperling, S. Ueberlein, M. Myndyk, G. Mäder, S. Kaskel, Formation of SiC nanoparticles in an atmospheric microwave plasma, Beilstein J. Nanotechnol. 2 (2011) 665–673.
[42] P. Rai, J.S. Park, G.G. Park, W.M. Lee, Y.T. Yu, S.K. Kang, S.Y. Moon, B.G. Hong, Influence of carbon precursors on thermal plasma assisted synthesis of SiC nanoparticles, Adv. Powder Technol. 25 (2014) 640–646.
[43] Z. Károly, I. Mohai, S. Klébert, A. Keszler, I.E. Sajó, J. Szépvölgyi, Synthesis of SiC powder by RF plasma technique, Powder Technol. 214 (2011) 300–305.
[44] L.R. Tong, R.G. Reddy, Thermal plasma synthesis of SiC nano-powders/nano-fibers, Mater. Res. Bull. 41 (2006) 2303–2310.
[45] J.Y. Guo, F. Gitzhofer, M.I. Boulos, Effects of process parameters on ultrafine SiC synthesis using induction plasmas, Plasma Chem. Plasma P 17 (1997) 219–249.

[46] (a) C. Czosnek, J.F. Janik, Particle morphology of various SiC-based nanocomposite powders made by the aerosol-assisted synthesis method, J. Nanosci. Nanotechnol. 8 (2008) 907–913;
(b) C. Czosnek, S. Kluska, J.F. Janik, Aerosol-assisted synthesis of SiC-based nanopowders from organosilicon precursor systems, Mater. Sci. -Poland 26 (2008) 309–318.
[47] M. Sitarz, C. Czosnek, P. Jeleń, M. Odziomek, Z. Olejniczak, M. Kozanecki, J.F. Janik, SiOC glasses produced from silsesquioxanes by the aerosol-assisted vapor synthesis method, Spectrochim. Acta A 112 (2013) 440–445.
[48] M. Bystrzejewski, A. Huczko, H. Lange, W.W. Płotczyk, R. Stankiewicz, T. Pichler, T. Gemming, M.H. Rümmeli, A continuous synthesis of carbon nanotubes by dc thermal plasma jet, Appl. Phys. A 91 (2008) 223–228.
[49] H. Bréquel, J. Parmentier, S. Walter, R. Badheka, G. Trimmel, S. Masse, J. Latournerie, P. Dempsey, C. Turquat, A. Desmartin-Chomel, L. Le Neindre-Prum, U.A. Jayasooriya, D. Hourlier, H.J. Kleebe, G.D. Sorarú, S. Enzo, F. Babonneau, Systematic structural characterization of the high-temperature behavior of nearly stoichiometric silicon oxycarbide glasses, Chem. Mater. 16 (2004) 2585–2598.
[50] M.A. Schiavon, S.U.A. Redondo, S.R.O. Pina, I.V.P. Yoshida, Investigation on kinetics of thermal decomposition in polysiloxane networks used as precursors of silicon oxycarbide glasses, J. Non-Cryst. Solids 304 (2002) 92–100.
[51] G.D. Sorarú, F. Babonneau, J.D. Mackenzie, Structural evolutions from polycarbosilane to SiC ceramic, J. Mater. Sci. 25 (1990) 3886–3893.